

Effects of Orthogonal Rotating Electric Fields on Electrospinning Process

F. Cipolletta¹, M. Lauricella¹, G. Pontrelli¹, D. Pisignano^{3,4}, and S. Succi^{1,2*}

¹*Istituto per le Applicazioni del Calcolo CNR, Via dei Taurini 19, 00185 Rome, Italy*

²*Harvard Institute for Applied Computational Science, Cambridge, Massachusetts 02138, United States*

³*Dipartimento di Matematica e Fisica Ennio De Giorgi,*

University of Salento, via Arnesano, 73100 Lecce, Italy and

⁴*Istituto Nanoscienze-CNR, Euromediterranean Center for Nanomaterial Modelling and Technology (ECMT), via Arnesano, 73100 Lecce, Italy*

(Dated: November 16, 2022)

Electrospinning is a nanotechnology process whereby an external electric field is used to accelerate and stretch a charged polymer jet, so as to produce fibers at nanoscale diameters. In quest of a further reduction in the cross section of electrified jets hence of the resulting electrospun fibers, we explore the effects of an external rotating electric field orthogonal to the jet direction. Through extensive particle simulations, it is shown that by a proper tuning of the electric field amplitude and frequency, a reduction of up to a 30% in the aforementioned radius can be obtained, thereby opening new perspectives in the design of future ultra-thin electrospun fibres.

Keywords: electrified jets, electric field, electrospinning, computational modelling, nanofibers.

Electrospinning has witnessed a dramatic upsurge of interest in recent years because of its potential to produce ultra-fine fibers with sub-micrometer diameters (see Refs [1–7]). Though routinely realizable in the laboratory, electrospinning is a complex phenomenon to analyse because of the coupling between the electric field and the non-linear deformation of the fluid, the latter being dictated by the rheology of the material. As a consequence, the resulting jet (fiber) diameter is affected by several material, design, and operating parameters. A significant source of information on the electrospinning process stems from observations, although the complexity of the process makes the empirical determination of parameter effects very demanding.

By using suitable theoretical models, the effects of the parameters on the fiber diameter can be systematically studied and evaluated, both analytically and numerically. For example, it has been shown that bending and whipping instabilities of electrical and hydrodynamical nature, are mostly responsible for jet stretching during the electrospinning process [8, 9]. This behaviour leads to a reduction of the cross section radius of electrospun nanofibers (Figure 1). In other studies, the attention is mostly focused on the morphological aspects, revealing a wide variety of pattern depositions of electrified jets [8, 10]. In the literature, one can find theoretical models to describe the jet dynamics and control the fiber diameter, through numerical simulations based on multi-parameter choice, involving the perturbation at the nozzle, the intensity of the fixed electric field, the density of polymer solution [9–12].

However, investigating new strategies to reduce the fiber diameter still is an open scientific and technological challenge. Applications enabled by producing ultra-thin fibers include chemical reactors working at extremely low

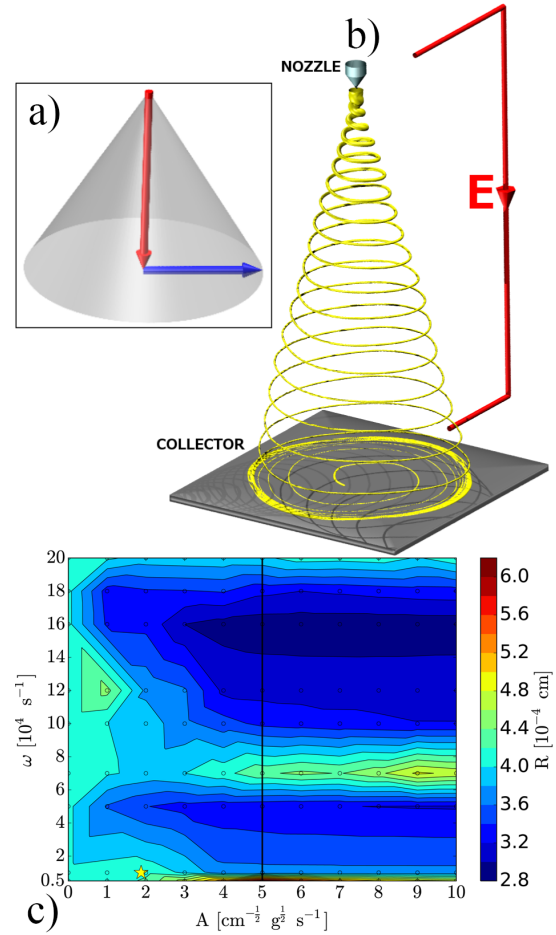


FIG. 1. Part A: Schematic representation of the axial (red) and orthogonal (blue) applied electric fields; Part B: Sketch representing the electrospinning process; Part C: Contour lines of the mean cross section radius R , computed for several values of $A \in [0, 10]$ and $\omega \in [0.5, 20]$ (circled points). The star indicates the reference values.

* Corresponding author: s.succi@iac.cnr.it

volumes [13], new schemes for nanophotonics and donor-acceptor energy transfer [14], and intracellular probing. On intuitive ground the longer the jet travels into the field, the more the instabilities have time to act on it thereby leading to the desired reduction of the jet cross section. Recently, the effect of a gas counter-flow has been numerically investigated [15]. On the other hand, it has been shown that a transverse electric field triggers additional instabilities that may radically change the jet dynamics and lead to the onset of jet breakup [8]. All the aforementioned investigations show that considering further effects within a classical electrospinning process, may drastically change the final result.

In the present Letter, we consider the effect of a rotating electric field orthogonal to the main electric field. In particular, we present a theoretical model and ensuing numerical simulations, in order to identify the optimal values of the amplitude and rotational frequency of the orthogonal rotating electric field (OREF) realising thinner electrospun fibers. The simulations have been performed with the public code JETSPIN [16–18]. More precisely, the jet emitted by the nozzle is represented by a finite set of n beads at a distance l_i (distance between the i th and $(i+1)$ th bead), connected each other via viscoelastic elements. From this representation, the following set of equations of motion (EOM) can be written for each bead i (hereafter, we shall consider the x -axis pointing from the nozzle to the collector):

$$\frac{d\vec{r}_i}{dt} = \vec{v}_i, \quad (1)$$

$$\frac{d\sigma_i}{dt} = \frac{G}{l_i} \frac{dl_i}{dt} - \frac{G}{\mu} \sigma_i, \quad (2)$$

$$m_i \frac{d\vec{v}_i}{dt} = q_i \vec{E} + \sum_{j \neq i} \left(\frac{q_i q_j}{|\vec{r}_j - \vec{r}_i|^2} \vec{u}_{i,j} \right) - \pi a_i^2 \sigma_i \vec{t}_i + \pi a_{i+1}^2 \sigma_{i+1} \vec{t}_{i+1} + k_i \pi \left(\frac{a_i + a_{i+1}}{2} \right)^2 \alpha \vec{c}_i, \quad (3)$$

In the above, subscript i stands for the i th bead, \vec{r}_i is the position vector, \vec{v}_i is the velocity vector, G is the elastic modulus, μ is the viscosity of the fluid jet, σ is the stress, a is the cross sectional radius, q is the charge, \vec{E} is the electric field (Figure 1), $\vec{u}_{i,j}$ is the unit vector from bead i to bead j , \vec{t}_i is the unit vector pointing from bead i to $(i-1)$, k is the local curvature, α is the surface tension coefficient and \vec{c}_i is the unit vector pointing from the bead i to the local centre of curvature [9].

The aforementioned system of EOM is solved, taking into account a periodic nozzle perturbation with frequency ω_{pert} and amplitude A_{pert} , which models fast oscillations nearby the spinneret. This perturbation results in the emission of a conic helix jet (see Table 1). Typical values of the main input parameters are reported in Tab. I (see [16] for details). We are interested in adding

TABLE I. Parameters values in the simulations.

simulated time	0.1	s
charge density	$4.4 \cdot 10^4$	$g \frac{1}{2} cm^{-\frac{3}{2}} s^{-1}$
fluid viscosity μ	20	$g cm^{-1} s^{-1}$
elastic modulus G	$5 \cdot 10^4$	$g cm^{-1} s^{-2}$
collector distance h	16	cm
external electric potential (hE^{\parallel})	30.021	$g \frac{1}{2} cm^{\frac{1}{2}} s^{-1}$
surface tension α	21.13	$g s^{-2}$
perturbation frequency ω_{pert}	10^4	s^{-1}
perturbation amplitude A_{pert}	10^{-3}	cm
OREF modulus A	[0.0, 10.0]	$g \frac{1}{2} cm^{-\frac{1}{2}} s^{-1}$
OREF frequency ω	[0.5, 20.0]	$10^4 s^{-1}$

an OREF to the above configuration, namely:

$$\vec{E} = \vec{E}^{\parallel} + \vec{E}^{\perp}. \quad (4)$$

Hereafter, the main electric field and the OREF are denoted by $\vec{E}^{\parallel} = (E_x, 0, 0)$ and $\vec{E}^{\perp} = (0, E_y, E_z)$, respectively. In equations:

$$\begin{aligned} E_y(A, \omega, t) &= A \cos \omega t, \\ E_z(A, \omega, t) &= A \sin \omega t, \end{aligned} \quad (5)$$

where $A(g \frac{1}{2} cm^{-\frac{1}{2}} s^{-1})$ is the modulus, $\omega(s^{-1})$ is the frequency. OREFs have already been treated in the literature, in the context of plasma confinement by means of a series of capacitor plates with alternating current, set around the apparatus [19]. In JETSPIN, we modified the EOM according to equation (4)–(5).

We investigate the effect of \vec{E}^{\perp} in equations (5), compared to the standard case \vec{E}^{\parallel} , and study the way that the jet morphology is deformed for different choices of the free-parameters. We take $A^* = |\vec{E}^{\parallel}| \simeq 1.8763$ and $\omega^* = \omega_{\text{pert}} = 10^4$ as reference values, respectively for A and ω in equations (5). A wide range of physically relevant values of these parameters is spanned by selecting $A \in [0, 10]$ and $10^{-4} \omega \in [0.5, 20]$ (see Ref. [20]). Such high values of the frequency ω mediate the OREF along the circumference orthogonal to \vec{E}^{\parallel} . Note that the dominant component of the force acting on each bead is the one given by \vec{E}^{\parallel} , since the jet travels towards the collector without undergoing any breakup, such as the one reported [8].

The two components of the electric field are shown in the top left panel of Figure 1, where the red and blue arrows represent \vec{E}^{\parallel} and \vec{E}^{\perp} , respectively, while the total field \vec{E} runs over the transparent grey conic surface. Results of simulations for the mean value of the cross section radius R at the collector are shown by contour lines in the bottom panel of Figure 1. Each process is simulated for a total time of 0.1s and the mean value is computed taking into account every time frame, after an initial drift $t_{\text{drift}} = 0.02s$, so that the jet dynamics is assumed regular [16]. It is worth observing that for $A = 0$ the mean cross section radius reduces to $R_0 = 4.05 \cdot 10^{-4}$,

in agreement with the mean cross section values obtained for the standard case, $\vec{E} = \vec{E}^{\parallel}$. As a representative value, we analyse the case $A = 5$ in Figure 2, namely the black vertical line in Figure 1. Along such line, we plot R as a function of ω , together with the corresponding confidence interval (namely the interquartile interval). In this figure, the thick black horizontal line indicates R_0 so as to allow a direct comparison between the cases with and without OREF.

From this plot, an oscillatory behaviour of R as a function of ω is clearly recognizable. Two representative points are singled out, namely the first minimum m_1 , with $R(m_1) = 2.65 \cdot 10^{-4}$, corresponding to $\omega(m_1) = 2.5 \times 10^4$, and the relative maximum M_1 with $R(M_1) = 4.15 \cdot 10^{-4}$, with $\omega(M_1) = 6 \times 10^4$. The shapes of the corresponding jet-path are reported in the sub-panels: one is the view from the side and the other is the view from the collector, looking up to the nozzle. It is worth noting that, although the helix associated with $\omega(M_1)$ is wider than the one for $\omega(m_1)$, the latter is more entangled, meaning that the jet undergoes longer-lived instabilities, resulting in a smaller value of R . 3D representations of the two highlighted trajectories are displayed in Figure 3, with color convention as stated in the caption of Figure 2. A reduction of the cross-section by about 34% with respect to case without OREF (namely $A = 0$ in Figure 1 for which R_0 is reported) is observed.

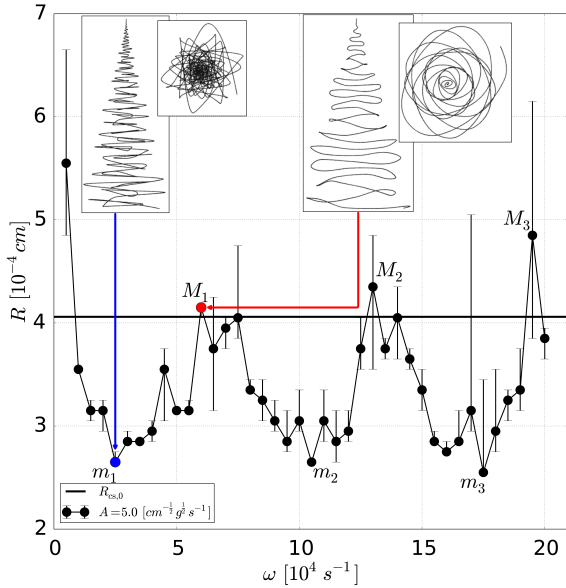


FIG. 2. Mean of cross section radius R at the collector for $A = 5$ at several values of ω , plotted with their respective interquartile as confidence intervals. The thick solid black horizontal line represents R_0 , i.e. the mean value of R in a standard electrospinning process (without OREF). The first minimum and maximum of R are highlighted in red, with the insets showing the shape of their trajectory from the lateral and bottom planes.

Even though the functional relation $R = R(\omega)$ is the

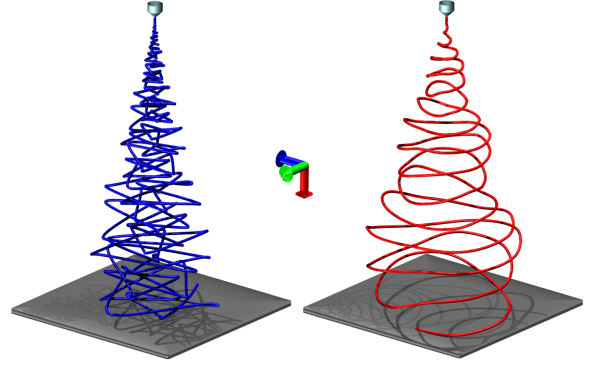


FIG. 3. Jet trajectories with $A = 5$, $\omega(m_1) = 2.5 \cdot 10^4$ (left blue curve) and $\omega(M_1) = 6 \cdot 10^4$ (right red curve). Axis convention, shown in the center, is as follows: red for x axis, green for y axis and blue for z axis. While the red curve is wider than the blue one, the latter appears more twisted, thus producing a thinner R (cfr with fig. 2 and 3).

result of a highly complex structural dynamics, the oscillatory structure of such relation is relatively regular, and suggestive of a sort of resonant mechanism underlying the OREF setup. At the moment, however, we have no clear theoretical explanation for such oscillatory behaviour, surely complicated by the specific rheology of the jet which responds non-linearly to the dynamical stretch impressed by the electric fields.

Each jet trajectory is the result of a complex dynamics, which presents an initial drift in the time lapse where the filament has not yet reached the collector (see caption of Figure 1). After such time lapse, the trajectory regularizes and consequently it becomes possible to analyse the statistical distribution of the cross section radius.

Figure 4 shows normalised histograms for the distribution of cross section radius at the collector for three different frequencies, $\omega = [2.5, 5.5, 6] \cdot 10^4$, all with the same amplitude $A = 5$.

It is apparent that the frequency distribution is skewed and strongly non Gaussian, which is relatively unsurprising due to the highly non-linear nature of the process. Owing to this non-Gaussianity, this observable is best described via its median and confidence interval (given by the first and third quartiles), as reported in Figure 2.

To gain further insights into the jet dynamics, it is also of interest to assess the "morphological distance" between two spirals corresponding to minimum and maximum fiber radii. Instead of a "smooth" Euclidean distance, we find it more informative to introduce an overlap distance between two trajectories α and β by taking cues from order parameters usually exploited in the context of glassy materials (see [21–23], which is defined as follows :

$$Q_{\alpha\beta}(t, \varepsilon) = \int_0^1 \Theta(\varepsilon - |\vec{r}_\alpha(t, \lambda) - \vec{r}_\beta(t, \lambda)|) d\lambda, \quad (6)$$

In the above, λ is the curvilinear coordinate, Θ the

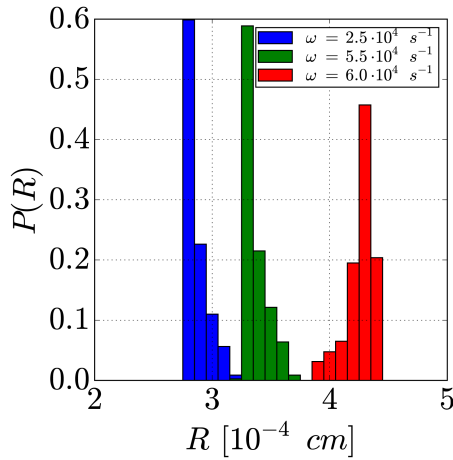


FIG. 4. Normalized histograms for distribution of cross section radius at the collector for $A = 5$ and several values of ω . These histograms show that the distribution of the observable during the dynamics is strongly skewed and non-gaussian.

Heaviside step function, ε (cm) a *distance* threshold. The Heaviside step function acts like a switch, turning off whenever the distance of the two jets at a certain λ is above a given threshold ε . Therefore $Q_{\alpha\beta}$ serves as a suitable indicator of the *separation transition* between two indistinguishable ($Q = 1$) and two fully separated ($Q = 0$) configurations, at the given scale ε . Note that by assuming the jet discretised as a set of n parcels (beads), each of them can only contribute a factor $1/n$ to the overlap parameter. This is in contrast with the euclidean distance which may eventually be completely dominated by a single, localised, large deviation between the two jets. Being sensitive to the value of ε , Q is a useful indicator of the dynamics of the separation process at different scales.

We evaluated the overlap distance for several values of the parameter ε as a function of time t , and correlate this indicator with $R(M_1)$ and $R(m_1)$. As a reference value, we take $\varepsilon_{\text{ref}} = 0.94\text{cm}$, i.e. the pitch distance for the jet-path in the case of R^{m_1} (see sub-panel of Figure 2). Our results pertain to $\alpha \equiv m_1$ and $\beta \equiv M_1$, in Figure 5, where a separation transition between the two jets is apparent. By definition, for $\varepsilon = 0$, the two jets are always separated, so that $Q_{m_1 M_1} = 0$ at all times.

On the other hand, at increasing ε , the two jets appear overlapped only up to an initial time t_{ov} , while for $t > t_{ov} \sim 0.01\text{s}$, a separation transition starts to take place, with the two jets getting more separated as ε is made smaller. After $t = 0.15\text{s}$, the distance between the two configurations reaches its asymptotic value. In Figure 6, we report some snapshots of the two jets at a given time, to provide a visual counterpart of the corresponding values of $Q_{m_1 M_1}(t, \varepsilon)$.

Summarising, we have proposed the OREF mechanism

and explored its effects on the electrospinning process, particularly on the diameter of the electrospun fibers, which can be reduced up to a 30%. Despite the inherent complexity of the underlying dynamics, the electrospin-

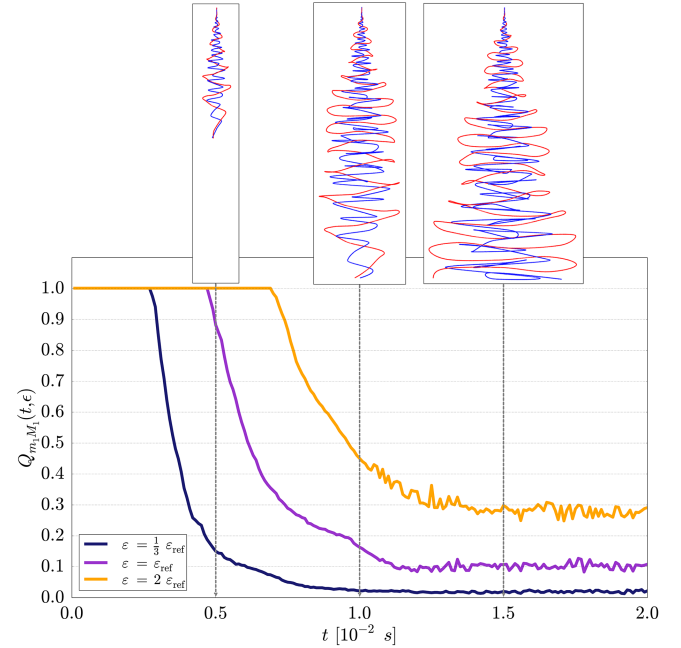


FIG. 5. Overlapping function $Q_{m_1 M_1}(t, \varepsilon)$ as a function of time, for three value of ε . For non-zero values of ε , an abrupt transition is evident, which stops after the drift time t_{drift} has been reached. In particular, the smaller the value of ε , the smaller $Q(\varepsilon, t)$ is. Snapshots of the two jets analysed at three times are reported at the insets over the plot, where colour legend is the same as Fig. 3.

ning response to OREF $R = R(\omega)$ appears to organise into a rather regular oscillatory pattern, with periodic local minima and maxima of the finer radius as a function of the OREF frequency. The existence of such minima opens up the possibility of advancing electrospinning technologies and producing finer fibers with high repeatability. Moreover, our simulations permit to highlight the salient morpho-dynamical features associated with the aforementioned minima and maxima in the electrospinning response.

Much remains to be done for the future; particularly, the study of the spatial dependence of the self-consistent electrostatic field induced by charge deposition at the collector, and its effects on the overall jet dynamics and associated deposition patterns. Current studies along these lines are under way.

The research leading to these results has received funding from the European Research Council under the European Union's Seventh Framework Programme (FP/2007-2013)/ERC Grant Agreement n. 306357 (NANO-JETS).

- ternational Edition **46**, 5670 (2007).
- [3] C. P. Carroll and Y. L. Joo, Journal of non-Newtonian fluid mechanics **153**, 130 (2008).
 - [4] Z.-M. Huang, Y.-Z. Zhang, M. Kotaki, and S. Ramakrishna, Composites science and technology **63**, 2223 (2003).
 - [5] A. L. Yarin, B. Pourdeyhimi, and S. Ramakrishna, *Fundamentals and Applications of Micro and Nanofibers* (Cambridge University Press, 2014).
 - [6] J. H. Wendorff, S. Agarwal, and A. Greiner, *Electrospinning: materials, processing, and applications* (John Wiley & Sons, 2012).
 - [7] D. Pisignano, *Polymer Nanofibers: Building Blocks for Nanotechnology*, 29 (Royal Society of Chemistry, 2013).
 - [8] W. Yang, H. Duan, C. Li, and W. Deng, Physical review letters **112**, 054501 (2014).
 - [9] D. H. Reneker, A. L. Yarin, H. Fong, and S. Koombhongse, Journal of Applied physics **87**, 4531 (2000).
 - [10] D. H. Reneker and A. L. Yarin, Polymer **49**, 2387 (2008).
 - [11] I. Coluzza, D. Pisignano, D. Gentili, G. Pontrelli, and S. Succi, Physical Review Applied **2**, 054011 (2014).
 - [12] S. V. Fridrikh, H. Y. Jian, M. P. Brenner, and G. C. Rutledge, Physical review letters **90**, 144502 (2003).
 - [13] P. Anzenbacher and M. A. Palacios, Nature chemistry **1**, 80 (2009).
 - [14] A. Camposeo, L. Persano, and D. Pisignano, Macromolecular Materials and Engineering **298**, 487 (2013).
 - [15] M. Lauricella, D. Pisignano, and S. Succi, The Journal of Physical Chemistry A (2016), 10.1021/acs.jpca.5b12450.
 - [16] M. Lauricella, G. Pontrelli, I. Coluzza, D. Pisignano, and S. Succi, Computer Physics Communications **197**, 227 (2015).
 - [17] M. Lauricella, G. Pontrelli, I. Coluzza, D. Pisignano, and S. Succi, Mechanics Research Communications **69**, 97 (2015).
 - [18] M. Lauricella, G. Pontrelli, D. Pisignano, and S. Succi, Molecular Physics **113**, 2435 (2015).
 - [19] X.-P. Huang, F. Anderegg, E. Hollmann, C. Driscoll, and T. O'neil, Physical Review Letters **78**, 875 (1997).
 - [20] M. Montinaro, V. Fasano, M. Moffa, A. Camposeo, L. Persano, M. Lauricella, S. Succi, and D. Pisignano, Soft matter **11**, 3424 (2015).
 - [21] M. Ozawa, W. Kob, A. Ikeda, and K. Miyazaki, Proceedings of the National Academy of Sciences **112**, 6914 (2015).
 - [22] W. Kob and L. Berthier, Physical review letters **110**, 245702 (2013).
 - [23] T. Kirkpatrick, D. Thirumalai, and P. G. Wolynes, Physical Review A **40**, 1045 (1989).